Structure and properties of ZnO/ZnMn$_2$O$_4$ composite obtained by thermal decomposition of terephthalate precursor

LIDIJA RADOVANOVIĆ[1*#], ŽELJKO RADOVANOVIĆ[1#], BOJANA SIMOVIĆ[2#],
MILICA V. VASIĆ[3], BOJANA BALANČ[1], ALEKSANDRA DAPČEVIĆ[4#],
MIROSLAV DRAMIĆANIN[5] and JELENA ROGAN[4#]

[1]*Innovation Centre of the Faculty of Technology and Metallurgy, University of Belgrade, Karnegijeva 4, Belgrade, Serbia,* [2]*Institute for Multidisciplinary Research, University of Belgrade, Kneza Višeslava 1, Belgrade, Serbia,* [3]*Institute for Testing of Materials IMS, University of Belgrade, Bulevar vojvode Mišića 43, Belgrade, Serbia,* [4]*Faculty of Technology and Metallurgy, University of Belgrade, Karnegijeva 4, Belgrade, Serbia and* [5]*Vinča Institute of Nuclear Sciences, University of Belgrade, P.O. Box 522, Belgrade, Serbia*

Abstract: A biphasic [Mn(dipya)(H$_2$O)$_4$](tpht)/{[Zn(dipya)(tpht)]·H$_2$O}$_n$ complex material, **I** (dipya = 2,2'-dipyridylamine, tpht^{2-} = dianion of terephthalatic acid) was synthesized by ligand exchange reaction and characterized by XRPD and FTIR spectroscopy. A ZnO/ZnMn$_2$O$_4$ composite, **II**, has been prepared *via* thermal decomposition of **I** in an air atmosphere at 450 °C. XRPD, FTIR and FESEM analyses of **II** revealed the simultaneous presence of spherical nanoparticles of wurtzite ZnO and elongated nanoparticles of spinel ZnMn$_2$O$_4$. The specific surface area of **II** was determined by the BET method, whereas the volume and average size of the mesopores were calculated in accordance with the BJH method. The measurements of the mean size, polydispersity index and zeta potential showed colloidal instability of **II**. Two band gap values of 2.4 and 3.3 eV were determined using UV–Vis diffuse reflectance spectroscopy, while the measurements of photoluminescence revealed that **II** is active in the blue region of the visible spectrum. Testing of composite **II** as a pigmentary material showed that it can be used for the colouring of a ceramic glaze.

Keywords: zinc(II)/manganese(II) complex; 1,4-benzenedicarboxylate; thermolysis; zincite; hetaerolite.

INTRODUCTION

Metal oxides and mixed metal oxides belong to the largest and most useful class of solid materials which have been extensively studied from various aspects

---

due to structural, compositional and functional diversities.[1,2] Zinc oxide (ZnO, zincite) is a multifunctional material with excellent properties, such as high chemical, thermal and mechanical stability, low toxicity, as well as high photostability, which is why it has been used in ceramics, medicine and photocatalysis.[3] Zinc manganese oxide ($ZnMn_2O_4$, hetaerolite) with spinel structure has been widely known for its magnetic, electronic or catalytic properties.[4] During the last decades the search for new materials that can be used as inorganic pigments is in grow, with a special emphasis on environmental suitability.[5,6] Inorganic pigments are important materials for colouring glazes, ceramics, plastics and glasses, owing to their high opacity, thermal stability and chemical resistance.[7] ZnO is a non-toxic alternative for lead white,[8] while $ZnMn_2O_4$, obtained from spent alkaline batteries, is suitable as brown pigment.[9]

Transition metal (TM) complexes with the anion of 1,4-benzenedicarboxylic (terephthalatic, H_2tpht) acid are functional materials with numerous applications in chemistry and material science.[10] The usage of the $tpht^{2-}$ anion as a linker between metal centres can result in the formation of fascinating supramolecular topologies because of diversity of coordination modes ranging from monodentate to even dodecadentate.[11,12] Until now, a vast number of TM–tpht compounds with different nuclearity and dimensionality, have been prepared and characterized, with many of them having tpht as a bridging ligand.[13] The possibility of using TM complexes as single-source precursors for obtaining functional oxide and mixed metal oxide nanomaterials by the direct thermal decomposition process has been assessed lately.[14,15] This approach, compared with the conventional synthetic methods, has several advantages such as the possibility of stoichiometry control and homogeneity from both aspects, in terms of metals distribution as well as in the terms of size and morphology of nanoparticles of obtained oxides.[14]

As a contribution to our previous research[16] relating the design and synthesis of mono- and heteronuclear TM complexes to prepare new functional materials, here we presented the synthesis, spectral and structural properties of a new biphasic Mn/Zn complex precursor (I) composed of coordination compounds $[Mn(dipya)(H_2O)_4](tpht)$ and $\{[Zn(dipya)(tpht)]\cdot H_2O\}_n$ (dipya = 2,2'-dipyridylamine), whose crystal structures have been described previously.[17,18] Following the preparation of the oxide nanomaterials by solid-state thermal decomposition of TM complexes, the biphasic complex **I** has been used as a single-source precursor for the synthesis of a composite powder **II** containing ZnO and $ZnMn_2O_4$. The structural, spectral, morphological, optical and photoluminescence properties of **II** have been investigated, as well as the possibility of using this material as a pigment.

EXPERIMENTAL

Materials

Except for dipya, which was of purum quality, all reagents were of analytical grade and used without further purification.

Synthesis of biphasic Mn/Zn complex precursor (I)

A solution of dipya (0.34 g, 2.0 mmol) in 7.5 cm^3 of EtOH was added into solution prepared by diluting a mixture of 1.0 M Mn(NO$_3$)$_2$ (1.0 cm^3, 1.0 mmol) and 1M Zn(NO$_3$)$_2$ (1.0 cm^3, 1.0 mmol) by 50 cm^3 of distilled water. Then, 25 cm^3 of an aqueous solution of Na$_2$tpht (10 cm^3, 2.0 mmol) was added dropwise at room temperature under continuous magnetic stirring. The obtained (beige) microcrystalline precipitate was filtered off after standing overnight, washed with small amounts of distilled water, EtOH and Et$_2$O and dried at room temperature.

Solid-state synthesis of ZnO/ZnMn$_2$O$_4$ composite (II)

The ZnO/ZnMn$_2$O$_4$ composite (II) has been obtained by the thermal degradation of precursor I in the air atmosphere. The mass of 0.45 g of I was heated at the constant rate up to 150 °C, isothermally calcinated at 150 °C for 30 min, then heated at the constant rate up to 450 °C, and isothermally calcinated at 450 °C during 1 h, and finally, spontaneously cooled to the room temperature. Yield: 19 %.

Measurements

The X-ray powder diffraction (XRPD) measurements for I and II were performed on a Rigaku SmartLab diffractometer using Cu$K\alpha$ radiation, at 40 kV and 30 mA, in Bragg––Brentano geometry. Diffraction data were collected in the range $3° < 2\theta < 120°$ (scan speed: $1°$ min^{-1}, step width: $0.01°$) for I and in the range $10° < 2\theta < 70°$ (scan speed: $1°$ min^{-1}, step width: $0.01°$) for II at room temperature. The crystal structure refinement of I and II was obtained by the full structure matching mode of the Rietveld refinement technique,[19] using the FULLPROF software.[20] The average crystallite size ($<D>$) for II was calculated using the Rigaku PDXL2 software and the whole powder pattern fitting (WPPF) method.

ATR-FTIR spectra of I and II were recorded in absorbance mode using a Nicolet™ iS™ 10 FTIR spectrometer (Thermo Fisher Scientific) with Smart iTR™ ATR sampling accessories, within the range of 4000–400 cm^{-1}, at a resolution of 4 cm^{-1} and in 20 scan mode.

Field emission scanning electron microscopy (FESEM) Tescan Mira 3 XMU was used for the morphological characterization of II. Using Mira software, the micrographs were analysed and the average diameters of the particles of II (more than 100 particles) were determined.

Diffuse reflectance UV–Vis spectrum for II was measured over the 200–800 nm spectral region (BaSO$_4$ was used as a reference standard) by Shimadzu UV-2600 spectrophotometer equipped with an integrating sphere.

The specific surface area (SSA) of II was calculated according to the Brunauer, Emmett and Teller (BET) method from the linear part of the nitrogen adsorption isotherm at 77 K on a Micrometrics ASAP 2020 instrument. Before the measurements, the samples were out-gassed at 150 °C for 10 h under a vacuum. The total pore volume (V_{tot}) was given at relative pressure $p/p_0 = 0.998$. The volume of the mesopores was calculated according to the Barrett, Joyner and Halenda (BJH) method from the desorption branch of the isotherm.

The mean size, polydispersity index (PDI) and zeta potential of II were measured by photon correlation spectroscopy and by electrophoretic light scattering using Zetasizer Nano

ZS (Malvern Instruments Ltd., Malvern, UK). The measurements were performed at the room temperature, and each sample was measured three times.

Photoluminescence (PL) measurements of **II** were performed at room temperature on Fluorolog-3 model FL3-221 spectrofluorimeter system (Horiba Jobin Yvon), utilizing a 450 W Xenon lamp as the excitation source for the steady-state measurements and xenon–mercury pulsed lamp for the time-resolved measurements. The emission spectrum of **II** was scanned in the range of wavelengths from 380 to 650 nm under 350 nm excitations. The TBX-04-D PMT detector was used for both time-resolved and steady state acquisitions. The line intensities and positions of the measured spectra were calibrated with a standard mercury–argon lamp. PL measurements were performed on pellets prepared from the powders under a pressure of 10 MPa.

To test the synthesized material **II** as a pigment for ceramic tiles glazing, several probes were done. The specimens in the shape of discs were prepared by dry hydraulic pressing of the raw clays ground to the fraction below 0.5 mm. The methodology is explained in more detail in the literature.[22] The specimens were dried to a constant mass in laboratory conditions. The blank transparent glaze was composed of ceramic glass frit in a quantity of 50 mass %, and the rest was distilled water. The freshly prepared batch was applied to the samples by immersing them in the mixture solution. The other probe consisted of the same glazing batch with the addition of 5 mass % of dried powder of pigment **II**. Both kinds of discs were dried overnight at 105 °C. The single-firing process was conducted in an oxidizing laboratory kiln using the usual regime for illitic-kaolinitic clays[21] to obtain a highly vitrified product.[22] The final firing temperature was set to 1200 °C based on preliminary probes with blank glazed samples. The chemical composition of the ceramic frit is obtained by energy dispersive X-ray fluorescence (XRF) using the Spectro Xepos instrument that contains 50 W/60 kV X-ray tube. The colour-space $L^*a^*b^*$ coordinates (L^* = lightness, a^* = saturation, b^* = intensity) of the obtained ceramic glazes were determined using a portable spectrophotometer ColorLite (SPH870) by a spectral scan in the steps of 7 recordings in 1 s. The certified white standard CL20602 is used as a reference. The obtained results showed values of L^*, a^* and b^*, providing information on red ($a^* > 0$) or green $a^* < 0$ and yellow ($b^* > 0$) or blue ($b^* < 0$) hues. The lightness of 0 is a standard of black, while 100 presents white colour. Glazed ceramic samples were recorded using a microscope at a magnification in the range of 40–400×. The samples were illuminated by an 1800 lm LED light source during shooting.

RESULTS AND DISCUSSION

*Characterization of precursor **I***

XRPD pattern for biphasic precursor **I** is presented in Fig. 1 and it showed that the system is composed of complexes [Mn(dipya)(H_2O)$_4$](tpht) and {[Zn(dipya)(tpht)]·H_2O}$_n$ (Table I and Fig. S-1 of the Supplementary material to this paper). The structural characterization of each phase was performed by the Rietveld method according to the known crystal structures of [Mn(dipya)(H_2O)$_4$](tpht) and {[Zn(dipya)(tpht)]·H_2O}$_n$ determined from the single crystal data.[17,18] The quantitative analysis showed that [Mn(dipya)(H_2O)$_4$](tpht):{[Zn(dipya)(tpht)]·H_2O}$_n$ phase-mass ratio was 31:69. The Rietveld refinement results (Tables I and S-I (Supplementary material)) displayed a minor deviation from the final structural parameters measured in the original structures.[17,18]
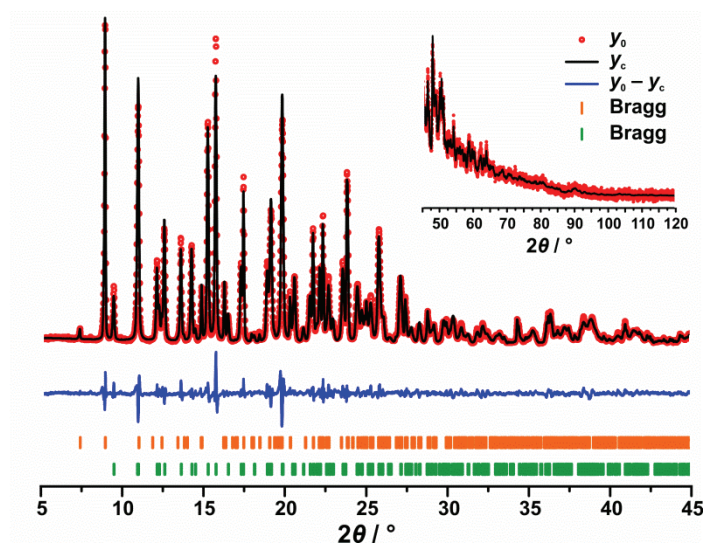
Fig. 1. Two-phased Rietveld refinement pattern of **I**. The Bragg positions of the [Mn(dipya)(H$_2$O)$_4$](tpht) and {[Zn(dipya)(tpht)]·H$_2$O}$_n$ phases are denoted by orange and green dashes, respectively.

TABLE I. Structural and fitting parameters obtained by Rietveld refinement for **I**

Phase	[Mn(dipya)(H$_2$O)$_4$](tpht)	{[Zn(dipya)(tpht)]·H$_2$O}$_n$
Crystal system	Monoclinic	Monoclinic
Space group	$P2_1/c$	$P2_1/n$
a / Å*	7.62706(8)	9.83335(13)
b / Å	23.8574(2)	14.40389(15)
c / Å	11.09296(19)	12.27168(15)
β / °	102.2957(10)	95.7916(9)
V / Å^3	1972.19(4)	1729.27(4)
R_B / %	2.39	3.15
R_f / %	1.99	3.16
Number of parameters refined	314	
R_{wp} / %	5.60	
R_p / %	4.28	
R_{exp} / %	4.42	
χ^2	1.60	

   The existence of water molecules, dipya and tpht ligands in **I** were confirmed from the FTIR spectrum shown in Fig. S-2 of the Supplementary material. A strong ν(O–H) stretching vibration at 3418 cm^{-1} corresponds to the lattice water molecules. Characteristic vibrations of the aromatic ring, ν(C=N) and ν(C=C), as well as ν(N–H) bands, are observed at 1659, 1483 cm^{-1} and in the

---

* 1 Å = 0.1 nm

3333–3207 cm^{-1} region, respectively, confirming the coordination of the dipya ligand. The presence of coordinated tpht caused the appearance of asymmetrical (ν_{as}) and symmetrical (ν_s) COO$^-$ vibrations at 1599 and 1385 cm^{-1}, respectively, while the vibrations found at 1639 and 1232 cm^{-1}, respectively, confirmed the presence of non-coordinated tpht ligand. In the fingerprint region, a strong peak positioned at 750 cm^{-1} is due to the presence of overlapped ν(N–H) and ν(C–H) vibrations.[23] A band ascribed to the ν(M–O) stretching vibration at 413 cm^{-1} verified the coordination of the water molecules as well as tpht ligands to the metal atom.[24]

*Characterization of composite **II***

The XRPD pattern of **II**, the calculated pattern, as well as the difference profile, are shown in Fig. 2. The Rietveld refinement revealed the coexistence of ZnO, which crystallizes in a hexagonal wurtzite structure and *P*6$_3$*mc* space group, and ZnMn$_2$O$_4$, which crystallizes in a tetragonal spinel structure and *I*4$_1$/*amd* space group. The quantitative phase fraction analysis revealed 62 mass % of ZnO phase and 38 mass % of ZnMn$_2$O$_4$ phase. The refined unit cell parameters (Table II) are in good agreement with PDF cards #36-1451 and #24--1123 for ZnO and ZnMn$_2$O$_4$ phases, respectively. The reliability factors of less than 5 % (Table II) pointed out that the experimental and calculated data are in good agreement. The calculated values of *<D>* for ZnO phase were similar in all directions meaning that its crystallites were almost spherical (Table II). The corresponding value for ZnMn$_2$O$_4$ phase along the *c*-axis was almost two times smaller than along *a*- and *b*-axes implying elongated crystallites of ZnMn$_2$O$_4$.
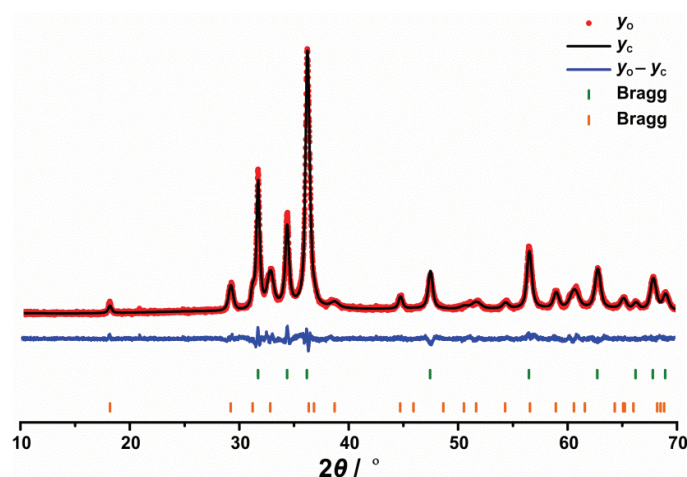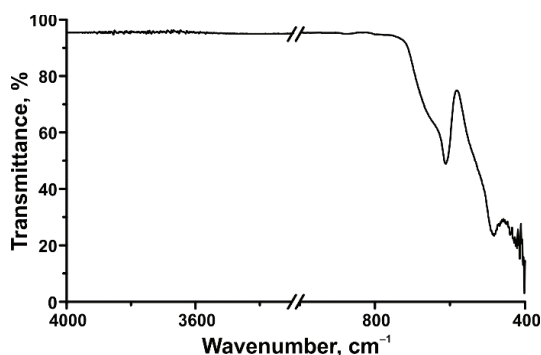

Fig. 2. Two-phase Rietveld refinement pattern of **II**. The Bragg positions of the ZnO and ZnMn$_2$O$_4$ phases are denoted by green and orange dashes, respectively.

The FTIR spectrum of **II** is presented in Fig. 3. The broad bands positioned at 611 and 483 cm^{-1} were ascribed to Mn–O stretching vibrations of MnO$_6$ octahedron, whereas the weak peaks observed in the region 424–402 cm^{-1} may be due to the presence of Zn–O bonds in ZnO$_4$ tetrahedral group.[25,26]

TABLE II. Structural and fitting parameters obtained by Rietveld refinement for **II**

Phase	ZnO	ZnMn$_2$O$_4$
Crystal system	Hexagonal	Tetragonal
Space group	$P6_3mc$	$I4_1/amd$
a / Å	3.2574(1)	5.7299(3)
c / Å	5.2175(2)	9.3000(8)
V / Å^3	47.945(3)	305.34(3)
$<D>$ / nm	26.5 [0,0,1];	19.5 [0,0,1]
	30.8 [–0.356,–0.935,0]	36.9 [–0.356,–0.935,0]
	30.8 [0.935,–0.356,0]	36.9 [0.935,–0.356,0]
Number of parameters refined	39	
R_{wp} / %	4.80	
R_p / %	3.82	
R_{exp} / %	3.80	
S	1.2633	
χ^2	1.5960	

Fig. 3. FTIR spectrum of **II**.

The FESEM micrographs of **II** are presented in Fig. 4. The powder is composed of deformed spherical nanoparticles of ZnO phase and the elliptical particles of ZnMn$_2$O$_4$ phase, which is in agreement with the results found by XRPD analysis. The FESEM micrograph made at higher magnification (Fig. 4b) shows that the particles of both phases have smooth surfaces with an average diameter of about 67 nm for ZnO phase and with average width and length of 156 and 290 nm, respectively, for ZnMn$_2$O$_4$ phase.

Zeta potential is very important for the stability of colloidal dispersions. In general, dividing line between stable and unstable dispersions is taken at ±30 mV. Particles with absolute zeta potentials higher than 30 mV are mainly considered stable.[27] The mean particle size was found to be (445.6±53.1) nm. This

can be explained by the formation of agglomerates which was also observed by FESEM. The value of zeta potential was (–7.80±0.86) mV, indicating that particles of **II** carried the negative surface charge and that colloidal dispersion is unstable. The estimated *PDI* was high with a value of 0.347±0.100, implying non-uniform dispersion of **II** during dyeing.[28–30]
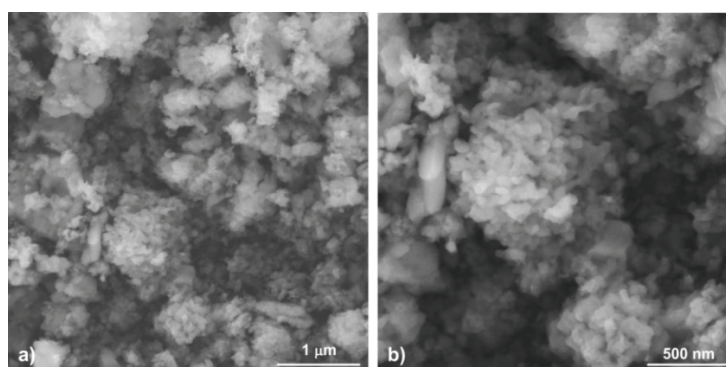

Fig. 4. FESEM images of **II** at different magnifications.

The results of the BET analysis of **II** are presented in Table III and Fig. 5. The value of *SSA* is small, being equal to 16.95 m^2 g^{-1}, while the average pore size was estimated to be 23.3 nm (Table III). Up to $p/p_0 = 0.8$, the slope of the N$_2$ adsorption/desorption isotherms of **II** is small due to the presence of a little number of small size pores (Fig. 5a). A slight separation of the adsorption and desorption isotherms of **II** was observed in the region 0.8–1 at p/p_0 axis, meaning that the quantity of micropores is also small, which further implied that pores were a consequence of the voids between the nanoparticles. The small *SSA* value of **II** denoted that composite could be uneven and weakened in colouring strength.[31]

TABLE III. The results of BET analysis of **II**; V_{tot} – total pore volume; V_{meso} – mesopore volume; V_{micro} – micropore volume; D_{aver} – average pore diameter; D_{max} – the diameter of the pores that occupy the largest part of the volume

SSA / m^2 g^{-1}	V_{tot} / cm^3 g^{-1}	V_{meso} / cm^3 g^{-1}	V_{micro} / cm^3 g^{-1}	D_{aver} / nm	D_{max}[a] / nm
16.95	0.0813	0.0772	0.0048	23.3	23.5 and 34.7

[a]Two maxima exist on the curve

The energy band gap (E_g) values for **II** were calculated from the plot of the modified Kubelka–Munk function $(F(R)h\nu)^2$ *vs.* the energy of the adsorbed light ($h\nu$) using the linear fits close to the absorption edge as it is shown in Fig. 6a. The absorption spectra exhibited double absorption edges and two different E_g values were determined: one at 2.4 eV and another at 3.3 eV. A lower E_g value could be ascribed to d–d transitions and the dark colour of **II**, as it is already observed for samples with a high concentration of TM in the structure, while a

higher E_g value could be due to an increase in the intensity of TM–O^{2-} charge transfer.[32] The steady-state emission spectrum of **II** obtained at room temperature is presented in Fig. 6b. Upon excitation at 350 nm, this analysis revealed a band centred at 422 nm in the blue region of the visible part of the spectrum followed by low or negligible absorption in the red and orange region, which is associated with the brown colour of **II**.[32]
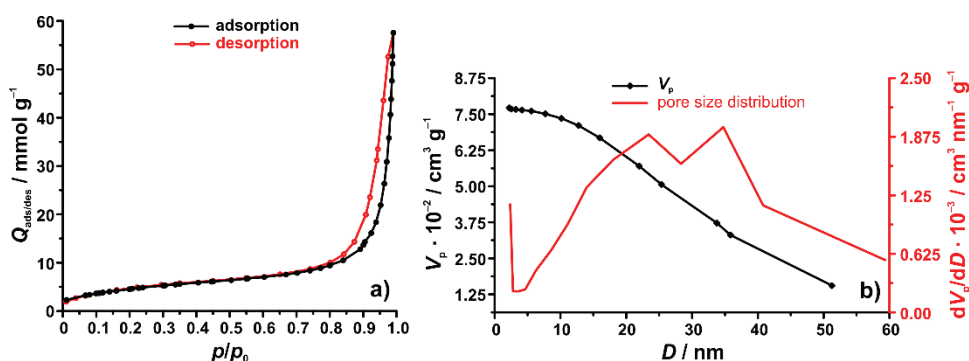

Fig. 5. Adsorption–desorption curves (a) and pore volume and pore size distribution (b) for **II**.
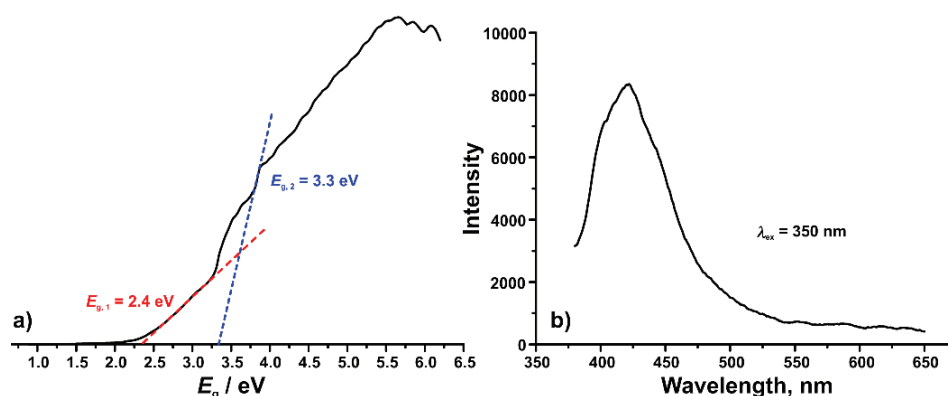

Fig. 6. Direct band gap energies (a) and the emission spectrum (b) of **II**.

The composite **II** is tested for application as a pigment for colouring the ceramic glaze. The transparent glaze is obtained from a glass frit containing a high quantity of SiO$_2$, and a high SiO$_2$/Al$_2$O$_3$ ratio (Table IV).

The low quantity of lead and absence of cadmium shows that the glaze is not toxic to living organisms.[33] The pigment material **II** was of a brownish–black colour with a value of L^* being 26.85 (Table V, Fig. 7a) and with a^* and b^* coordinates similar to other materials with spinel structure used as pigments.[6,32] The dark pigment decreased the lightness of the glaze by about 37 %, whereas, at the same time, redness and yellowness increased. In both transparent and pig-

322 RADOVANOVIĆ *et al.*

mented glazes, a smooth surface is obtained (Fig. 7b–c and Fig. S-3 of the Supplementary material). The unevenness of the pigment distribution may be caused by an insufficient quantity of the pigment particles that grouped and spread over the transparent glaze during the sintering process. In addition, unevenness of the pigment **II** is in accordance with its small value of *SSA* (Table III), high *PDI* and zeta potential close to zero.

TABLE IV. Chemical composition of the ceramic glass used for glazing; *LOI* – loss on ignition

Component	Share, %	Component	Share, %
LOI	3.47	SO_3	0.04
SiO_2	62.16	P_2O_5	0.06
Al_2O_3	15.76	MnO	0.00
Fe_2O_3	0.19	TiO_2	0.06
CaO	9.84	Pb	0.03
MgO	0.46	Cd	0.00
Na_2O	6.00	Ba	0.89
K_2O	0.92	Sum	99.87

TABLE V. CIE *L*a*b** colorimetric coordinates of the pigment **II** and glazes

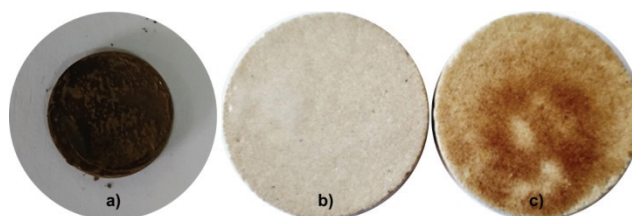| Sample	*L**	*a**	*b**
II	26.85	2.94	4.96
Transparent glaze	64.88	2.60	15.38
Pigmented glaze	40.70	11.26	22.04

Fig. 7. The appearance of the pigment **II** (a), transparent (b) and pigmented glazed ceramics (c).

The advantages of composite materials considered as not harmful to health may make these glazes promising and widely used on surfaces where glazed ceramics come into contact with food or chemicals.[34]

CONCLUSION

Direct solid-state decomposition of terephthalate precursor **I**, composed of 31 mass % of [Mn(dipya)(H_2O)$_4$](tpht) and 69 mass % of {[Zn(dipya)(tpht)]·H_2O}$_n$, gave as result the nanocrystalline ZnO/ZnMn$_2$O$_4$ brown composite material, **II**, with phase mass ratio of 68:32 for ZnO:ZnMn$_2$O$_4$. Rietveld structure refinement results revealed the presence of wurtzite ZnO and spinel ZnMn$_2$O$_4$. Particle size of ZnO phase was about 67 nm, while width and

length of $ZnMn_2O_4$ particles were about 156 and 290 nm, respectively. The *PDI* of 0.347, small value of *SSA* of 16.95 m^2 g^{-1} and zeta potential value of −7.80 mV resulted in unstable pigmentary dispersion of **II** and uneven distribution of pigment during dyeing of transparent ceramic glaze. Since the composite **II** is composed of nontoxic oxides, it is expected to be the environmentally safe for application as pigmentary material in paints, polymers and ceramics.

SUPPLEMENTARY MATERIAL

Additional data and information are available electronically at the pages of journal website: https://www.shd-pub.org.rs/index.php/JSCS/article/view/12126, or from the corresponding author on request.

И З В О Д

СТРУКТУРА И СВОЈСТВА КОМПОЗИТА ZnO/ZnMn₂O₄ ДОБИЈЕНОГ ТЕРМИЧКОМ РАЗГРАДЊОМ ТЕРЕФТАЛАТ-ПРЕКУРСОРА

ЛИДИЈА РАДОВАНОВИЋ[1], ЖЕЉКО РАДОВАНОВИЋ[1], БОЈАНА СИМОВИЋ[2], МИЛИЦА В. ВАСИЋ[3], БОЈАНА БАЛАНЧ[1], АЛЕКСАНДРА ДАПЧЕВИЋ[4], МИРОСЛАВ ДРАМИЋАНИН[5] и ЈЕЛЕНА РОГАН[4]

[1]Иновациони центар Технолошко–металуршког факултета, Универзитет у Београду, Карнегијева 4, Београд, [2]Институт за мултидисциплинарна истраживања, Универзитет у Београду, Кнеза Вишеслава 1, Београд, [3]Институт за испитивање материјала ИМС, Универзитет у Београду, Булевар војводе Мишића 43, Београд, [4]Технолошко–металуршки факултет, Универзитет у Београду, Карнегијева 4, Београд и [5]Институт за нуклеарне науке „Винча", Универзитет у Београду, Поштански преградак 522, Београд

Двофазни $[Mn(dipya)(H_2O)_4](tpht)/\{[Zn(dipya)(tpht)]\cdot H_2O\}_n$ комплексни материјал, **I**, (dipya = 2,2'-дипиридиламин, tpht^{2-} = дианјон 1,4-бензендикарбоксилне киселине) синтетисан је реакцијом измене лиганада и окарактерисан XRPD методом и FTIR спектроскопијом. Композит ZnO/ZnMn₂O₄, **II**, добијен је термичком разградњом прекурсора **I** у атмосфери ваздуха на 450 °C. XRPD методом, FTIR спектроскопијом и FESEM микроскопијом композита **II** утврђено је истовремено присуство сферних наночестица ZnO вирцитне структуре и издужених наночестица ZnMn₂O₄ са структуром спинела. Специфична површина композита **II** одређена је BET методом, док су запремина и просечна величина мезопора израчунати у складу са BJH методом. Средња величина, индекс полидисперзије и цета потенцијал измерени су фотонском корелационом спектроскопијом и електрофоретским расејањем светлости и показали су нестабилност композита **II**. Вредности ширине забрањене зоне од 2,4 и 3,3 eV одређене су UV–Vis дифузно-рефлексионом спектроскопијом, док су мерења фотолуминесценције показала да је композит **II** активан у плавој области видљивог дела спектра. Испитивање композита **II** као пигментног материјала показало је да се може користити за бојење керамичке глазуре.

(Примљено 2. новембра, ревидирано 17 децембра, прихваћено 21. децембра 2022)

REFERENCES

1. C. Yuan, H. B. Wu, Y. Xie, X. W. Lou, *Angew. Chem. Int. Ed.* **53** (2014) 1488 (https://dx.doi.org/doi: 10.1002/anie.201303971)
2. C. N. R. Rao, B. Raveau, *Transition Metal Oxides: Structure, Properties, and Synthesis of Ceramic Oxides*, 2nd ed., Wiley-VCH, New York, 1998 (https://doi.org/10.1002/(SICI)1099-0739(199906)13:6<476::AID-AOC851>3.0.CO;2-N)
3. A. Kołodziejczak-Radzimska, T. Jesionowski, *Materials* **7** (2014) 2833 (https://dx.doi.org/10.3390/ma7042833)
4. G. D. Park, Y. C. Kang, J. S. Cho, *Nanomaterials* **12** (2022) 680 (https://doi.org/10.3390/nano12040680)
5. M. Fortuño-Morte, P. Serna-Gallén, H. Beltrán-Mir, E. Cordoncillo, *J. Mat.* **7** (2021) 1061 (https://doi.org/10.1016/j.jmat.2021.02.002)
6. T. E. R. Fiuza, D. Göttert, L. J. Pereira, S. R. M. Antunes, A. V. C. de Andrade, A. C. Antunes, É. C. F. de Souza, *Process. Appl. Ceram.* **12** (2018) 319 (https://doi.org/10.2298/PAC1804319R)
7. G. Pfaff, *Phys. Sci. Rev.* **7** (2022) 7 (https://doi.org/10.1515/psr-2020-0183)
8. G. Osmond, *AICCM Bull.* **33** (2012) 20 (http://dx.doi.org/10.1179/bac.2012.33.1.004)
9. L. J. Almeidaa, E. C. Grzebieluckaa, S. R. M. Antunesa, C. P. F. Borgesa, A. V. C. de Andradeb, É. C. F. de Souza, *Mat. Res.* **23** (2020) e20190515 (https://doi.org/10.1590/1980-5373-MR-2019-0515)
10. T. R. Cook, Y. R. Zheng, P. J. Stang, *Chem. Rev.* **113** (2013) 734 (https://doi.org/10.1021/cr3002824)
11. D. Sun, R. Cao, Y. Liang, Q. Shi, W. Sua, M. Hong, *J. Chem. Soc., Dalton Trans.* (2001) 2335 (https://doi.org/10.1039/B102888J)
12. Z. Cheng, H. Shi, H. Ma, L. Bian, Q. Wu, L. Gu, S. Cai, X. Wang, W. Xiong, Z. An, W. Huang, *Angew. Chem. Int. Ed.* **57** (2018) 678 (https://doi.org/10.1002/anie.201710017)
13. C. R. Groom, I. J. Bruno, M. P. Lightfoot, S. C. Ward, *Acta Crystallogr., B* **72** (2016) 171 (https://doi.org/10.1107/S2052520616003954)
14. H. Lu, D. S. Wright, S. D. Pike, *Chem. Commun.* **56** (2020) 854 (https://doi.org/10.1039/C9CC06258K)
15. M. Y. Masoomi, A. Morsali, *Coord. Chem. Rev.* **256** (2012) 2921 (https://doi.org/10.1016/j.ccr.2012.05.032)
16. L. Radovanović, J. D. Zdravković, B. Simović, Ž. Radovanović, K. Mihajlovski, M. D. Dramićanin, J. Rogan, *J. Serb. Chem. Soc.* **85** (2020) 1475 (https://doi.org/10.2298/JSC200629048R)
17. L. Radovanović, J. Rogan, D. Poleti, M. V. Rodić, N. Begović, *Inorg. Chim. Acta* **445** (2016) 46 (https://doi.org/10.1016/j.ica.2016.02.026)
18. L. Radovanović, J. Rogan, D. Poleti, M. Milutinović, M. V. Rodić, *Polyhedron* **112** (2016) 18 (https://dx.doi.org/10.1016/j.poly.2016.03.054)
19. H. M. Rietveld, *J. Appl. Cryst.* **2** (1969) 65 (https://doi.org/10.1107/S0021889869006558)
20. J. Rodríguez-Carvajal, *Newsletter* **26** (2001) 12 (http://journals.iucr.org/iucr-top/comm/cpd/Newsletters/)
21. M. V. Vasić, L. Pezo, M. R. Vasić, N. Mijatović, M. Mitrić, *Bol. Soc. Esp. Ceram. V.* (2020) (https://doi.org/10.1016/j.bsecv.2020.11.006)
22. C. Molinari, S. Conte, C. Zanelli, M. Ardit, G. Cruciani, M. Dondi, *Ceram. Int.* **46** (2020) 21839 (https://doi.org/10.1016/j.ceramint.2020.05.302)
23. E. Castellucci, L. Angeloni, N. Neto, G. Sbrana, *Chem. Phys.* **43** (1979) 365 (https://doi.org/10.1016/0301-0104(79)85204-0)

24. K. Nakamoto, *Infrared and Raman Spectra of Inorganic and Organic Coordination Compounds*, Part B, 5th ed., Wiley-Interscience, New York, 1997
25. N. Senthilkumar, V. Venkatachalam, M. Kandiban, P. Vigneshwaran, R. Jayavel, Vetha Potheher, *Physica E* **106** (2019) 121 (https://doi.org/10.1016/j.physe.2018.10.027)
26. W. Konicki, D. Sibera, U. Narkiewicz, *Separ. Sci. Technol.* **53** (2018) 1295 (https://doi.org/10.1080/01496395.2018.1444054)
27. Holmberg, D. O. Shah, M. J. Schwuger, *Handbook of Applied Surface and Colloid Chemistry*, Vol. 2, John Wiley & Sons, Ltd., Chichester, 2002
28. R Greenwood, K Kendall, *J. Eur. Ceram. Soc.* **19** (1999) 479 (http://dx.doi.org/10.1016/S0955-2219(98)00208-8)
29. M. Staiger, P. Bowen, J. Ketterer, J. Bohonek, *J. Disper. Sci. Technol.* **23** (2002) 619 (https://doi.org/10.1081/DIS-120015367)
30. Nie, G. Chang, R. Li, *Coatings* **20** (2020) 741 (https://doi.org/10.3390/coatings10080741)
31. H. Morii, K. Hayashi, K. Iwasaki, (Hiroshima-shi, Hiroshima-ken (JP)), EP 1 686 158 B1 (2006)
32. E. A. Medina, J. Li, M. A. Subramanian, *Prog. Solid State Chem.* **45**–**46** (2017) 9 (https://doi.org/10.1016/j.progsolidstchem.2017.02.002)
33. SRPS EN ISO 10545-15: *Ceramic tiles — Part 15: Determination of lead and cadmium given off by glazed tiles*, 2012
34. J. W. Gallaway, M. Menard, B. Hertzberg, Z. Zhong, M. Croft, L. A. Sviridov, D. E. Turney, S. Banerjee, *J. Electrochem. Soc.* **162** (2015) A162 (https://doi.org/10.1149/2.0811501jes).